Earthquakes and Structures, Vol. 3, No. 3-4 (2012) 203-230
DOI: http://dx.doi.org/10.12989/eas.2012.3.3.203

Dynamic analysis of foundations in a layered half-space using a consistent transmitting boundary

Jin Ho Lee[1], Jae Kwan Kim[2] and John L. Tassoulas*[1]

[1]*Department of Civil, Architectural and Environmental Engineering, the University of Texas at Austin, Austin, Texas, USA*
[2]*Department of Civil and Environmental Engineering, Seoul National University, Seoul, Korea*

(Received July 11, 2011, Revised October 3, 2011, Accepted October 31, 2011)

Abstract. This paper presents results for impedance (and compliance) functions and input motions of foundations in a layered half-space computed on the basis of a procedure that combines a consistent transmitting boundary with continued-fraction absorbing boundary conditions which are accurate and effective in modeling wave propagation in various unbounded domains. The effects of obliquely incident seismic waves in a layered half-space are taken into account in the formulation of the transmitting boundary. Using the numerical model, impedance (and compliance) functions and input motions of rigid circular foundations on the surface of or embedded in a homogeneous half-space are computed and compared with available published results for verification of the procedure. Extrapolation methods are proposed to improve the performance in the very-low-frequency range and for the static condition. It is concluded from the applications that accurate analysis of foundation dynamics and soil-structure interaction in a layered half-space can be carried out using the enhanced consistent transmitting boundary and the proposed extrapolations.

Keywords: foundation dynamics; soil-structure interaction; consistent transmitting boundary; continued-fraction absorbing boundary condition; layered half-space; wave propagation

1. Introduction

The effects of soil-structure interaction can strongly influence the dynamic response of structures, especially massive, stiff ones, founded on relatively flexible ground. Accordingly, dynamic soil-structure interaction has been studied extensively. Formulations of the interaction for flexible structures supported on rigid or flexible foundations have been presented. One of the steps in the solution of dynamic soil-structure interaction problems is the evaluation of impedance (and compliance) functions and input motions (and driving forces) for surface or embedded foundations. For this purpose, the impedance (and compliance) functions for surface foundations of various shapes in various conditions have been calculated (Bougacha *et al.* 1993a, Bougacha *et al.* 1993b, Gazetas and Roësset 1976, Gazetas and Roësset 1979, Kausel *et al.* 1975, Lin *et al.* 1987, Luco and Westmann 1971, Luco and Westmann 1972, Wong 1975, Wong and Luco 1978a). Also, those for embedded foundations have been evaluated using various techniques (Apsel and Luco 1987, Day

*Corresponding author, Professor, E-mail: yannis@mail.utexas.edu

1977, Kausel and Roësset 1975). The input motions (and driving forces) for the surface and embedded foundations have been examined (Day 1977, Iguchi 1984, Luco and Mita 1987, Luco and Wong 1987, Pais and Kausel 1989, Wong and Luco 1978a, Wong and Luco 1978b). Various analysis techniques for foundation dynamics have been reviewed by Roësset (1980) and Luco (1982).

In this study, impedance functions and input motions of rigid cylindrical (or circular) foundations in a layered half-space are examined. Shown in Fig. 1(a) is a typical soil-structure system under consideration. Supported on a rigid or flexible foundation, the structure is placed on or embedded in layered soil that overlies a half-space. The layered soil on the half-space is divided into two regions. One is a near-field region which can be irregular in geometry and inhomogeneous in elastic properties. The other is the far-field region which is assumed to have a regular layered structure and homogeneous elastic properties in the horizontal direction. The irregular and inhomogeneous near-field region is usually modeled by conventional finite elements. On the other hand, the regular and homogeneous layered far-field region is represented by mathematical or numerical models that are capable of elastic-wave radiation into infinity. One of the most convenient and appropriate models for the far-field region is a consistent transmitting boundary (Bougacha *et al.* 1993a, Bougacha *et al.* 1993b, Kausel 1974, Kausel *et al.* 1975, Kausel and Roësset 1975, Lin *et al.* 1987, Tassoulas 1981, 1984, Waas 1972). The consistent transmitting boundary is built on a semi-analytic finite-element method. It relies on a discretization of the medium in the direction of layering while analytical solutions are used in the radial direction to infinity. Therefore, it is an appropriate numerical model for the layered system and can be easily applied to complex problems where the near-field region is represented using finite elements method. In addition, the fact that the consistent transmitting boundary is based on a synthesis of eigenmodes of the layered soil entails another computational advantage. Because of the modal synthesis, the evaluation of the necessary integral transforms between the spatial and wavenumber domains can be carried out exactly without numerical quadrature, thereby avoiding errors associated with either truncation or large and rapid oscillations of the kernels (Kausel 1996). On account of these strengths, the consistent transmitting boundary has been applied to problems of foundation dynamics successfully (Bougacha *et al.* 1993a, Bougacha *et al.* 1993b, Kausel 1974, Kausel *et al.* 1975, Kausel and Roësset 1975, Lin *et al.* 1987, Tassoulas 1981, 1984, Waas 1972).

The consistent transmitting boundary is versatile in problems of dynamics of a layered *stratum* of finite depth but requires special care when applied to problems in a layered *half-space*. In the latter applications, the energy of waves radiated by the structure is often assumed to be confined near the surface of the layered half-space and the half-space is replaced with a layered stratum on rigid bedrock at sufficient depth. However, the fixed boundary condition can lead to unsatisfactory results, especially at low frequencies, if the depth of the stratum is not sufficient. To overcome this difficulty, second-order paraxial approximations of exact half-space conditions and "continued-fraction absorbing boundary conditions" (CFABCs) have been implemented in order to enhance the performance of consistent transmitting boundaries (Andrade 1999, Lee *et al.* 2011a, 2011b, Lee and Tassoulas 2011). In particular, the CFABCs are arbitrarily high-order local absorbing boundary conditions, effective in modeling wave propagation in various unbounded domains. They are compatible with domain-based numerical tools such as finite elements and can be implemented to any desired degree of accuracy. A consistent transmitting boundary combined with the CFABCs was formulated in plane strain and applied to dynamics of rigid foundations on a layered half-space to verify its effectiveness by Lee and Tassoulas (2011).

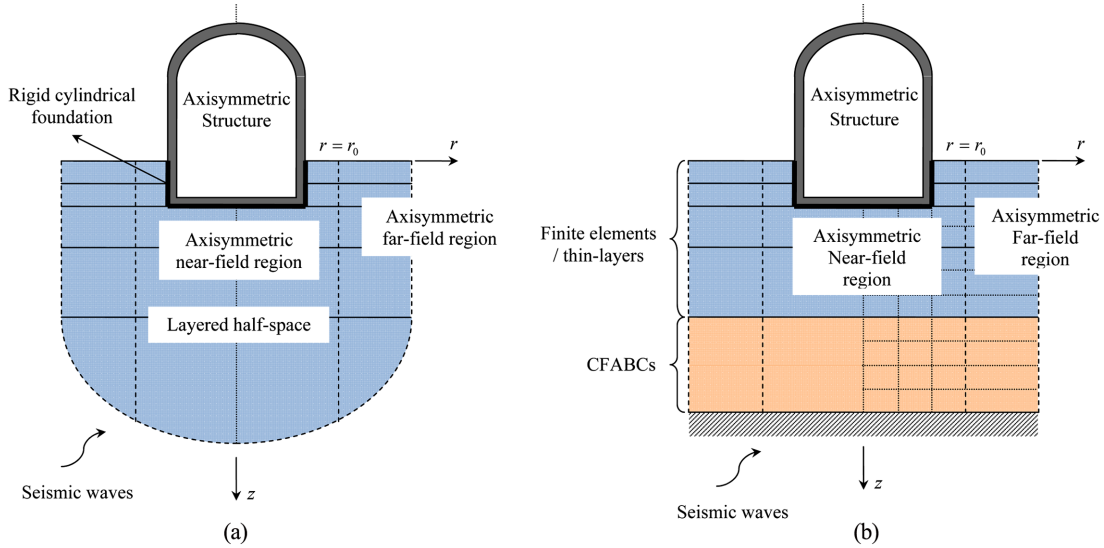

Fig. 1 Soil-structure system in a layered half-space: (a) schematic view and (b) numerical model

In this study, impedance functions and input motions of rigid cylindrical (or circular) foundations in a layered half-space are obtained using a consistent transmitting boundary combined with CFABCs. The outline of the paper is as follows. In Section 2, a consistent transmitting boundary with CFABCs will be formulated in a cylindrical coordinate system. In Section 3, the effects of obliquely incident seismic waves will be considered. The consistent transmitting boundary will be applied to dynamics of embedded circular foundations in a layered half-space to demonstrate and verify its accuracy in Section 4. Also, in Section 4, extrapolation methods will be proposed to improve behaviors of the numerical model in the very-low-frequency range and for the static condition. The paper will be summarized in Section 5.

2. Consistent transmitting boundary with continued-fraction absorbing boundary conditions

As mentioned in Section 1, the near-field region of a layered half-space is usually modeled by conventional finite elements and the far-field region by a consistent transmitting boundary. A formulation for the conventional finite elements for axisymmetric structures with asymmetric loads can be found in books on the finite element method. In this section, a consistent transmitting boundary combined with the CFABCs will be formulated in a cylindrical coordinate system to represent the far-field region of a layered half-space. Since the CFABCs are compatible with conventional finite elements, their implementation is similar. Hence, the formulation will be comparable to that for the consistent transmitting boundary without the CFABCs. The differences will be limited to the element matrices for the CFABCs.

An elastic wave equation in a cylindrical coordinate system can be written as follows (Kausel 1974)

$$(\lambda+2\mu)\frac{\partial \varepsilon}{\partial r}-\frac{2\mu}{r}\frac{\partial \omega_z}{\partial \theta}+2\mu\frac{\partial \omega_\theta}{\partial z}-\rho\ddot{u}_r=0 \tag{1a}$$

$$(\lambda+2\mu)\frac{\partial \varepsilon}{\partial z}-\frac{2\mu}{r}\frac{\partial(r\omega_\theta)}{\partial r}+\frac{2\mu}{r}\frac{\partial \omega_r}{\partial z}-\rho\ddot{u}_z=0 \tag{1b}$$

$$(\lambda+2\mu)\frac{1}{r}\frac{\partial \varepsilon}{\partial \theta}-2\mu\frac{\partial \omega_r}{\partial z}+2\mu\frac{\partial \omega_z}{\partial r}-\rho\ddot{u}_\theta=0 \tag{1c}$$

where

$$\varepsilon=\frac{1}{r}\frac{\partial(ru_r)}{\partial r}+\frac{1}{r}\frac{\partial u_\theta}{\partial \theta}+\frac{\partial u_z}{\partial z} \tag{2a}$$

$$\omega_r=\frac{1}{2}\left(\frac{1}{r}\frac{\partial u_z}{\partial \theta}-\frac{\partial u_\theta}{\partial z}\right) \tag{2b}$$

$$\omega_z=\frac{1}{2}\left(\frac{\partial(ru_\theta)}{\partial r}-\frac{\partial u_r}{\partial \theta}\right) \tag{2c}$$

$$\omega_\theta=\frac{1}{2}\left(\frac{\partial u_r}{\partial z}-\frac{\partial u_z}{\partial r}\right) \tag{2d}$$

In Eqs. (1) and (2), u_r, u_z and u_θ denote the radial, axial and tangential displacements, respectively, λ and μ Lamé constants, and ρ the density.

Assuming time-harmonic motion of frequency ω, solutions of Eq. (1) are obtained by the method of separation of variables (Kausel 1974, Tassoulas 1981). The solutions correspond to motions in plane strain and antiplane shear as follows

$$u_r(r,\theta,z)=kU_x(z)C_m'(kr)\begin{bmatrix}\cos(m\theta)\\ \sin(m\theta)\end{bmatrix} \tag{3a}$$

$$u_z(r,\theta,z)=-ikU_z(z)C_m(kr)\begin{bmatrix}\cos(m\theta)\\ \sin(m\theta)\end{bmatrix} \tag{3b}$$

$$u_\theta(r,\theta,z)=\frac{m}{r}U_x(z)C_m(kr)\begin{bmatrix}-\sin(m\theta)\\ \cos(m\theta)\end{bmatrix} \tag{3c}$$

and

$$u_r(r,\theta,z)=\frac{m}{r}U_y(z)C_m(kr)\begin{bmatrix}\cos(m\theta)\\ \sin(m\theta)\end{bmatrix} \tag{4a}$$

$$u_z(r,\theta,z)=0 \tag{4b}$$

$$u_\theta(r,\theta,z)=kU_y(z)C_m'(kr)\begin{bmatrix}-\sin(m\theta)\\ \cos(m\theta)\end{bmatrix} \tag{4c}$$

In Eqs. (3) and (4), k is a wavenumber, $U_x(z)$ and $U_z(z)$ are wave modes in plane strain, and $U_y(z)$ is a wave mode in antiplane shear, m is the Fourier number, $C_m(kr)$ is any solution of the Bessel equation of order m and the prime denotes differentiation with respect to the argument kr. The upper terms in the square brackets are for the symmetric modes and the lower terms for the anti-

symmetric modes. It can be shown by substitution that the expressions in Eq. (3) are solutions to Eq. (1) provided that $U_x(z)$ and $U_z(z)$ satisfy the governing equations for the wave modes in plane strain (Tassoulas 1981). Analogously, the expressions in Eq. (4) are solutions to Eq. (1), if $U_y(z)$ is a wave mode in antiplane shear.

The wavenumber and wave modes in Eqs. (3) and (4) are computed from eigenvalue problems in plane strain and antiplane shear (Kausel 1974, Tassoulas 1981). Using the finite-element approach, the following algebraic eigenvalue problems are obtained

$$[k^2\mathbf{A} + ik\mathbf{B} + \mathbf{G} - \omega^2\mathbf{M}]\Delta = \mathbf{0} \text{ in plane strain} \tag{5a}$$

$$[k^2\mathbf{A} + \mathbf{G} - \omega^2\mathbf{M}]\Delta = \mathbf{0} \text{ in antiplane shear} \tag{5b}$$

where Δ is the corresponding eigenvector. For ordinary layers of sufficiently small thickness with linear displacement interpolation, the matrices **A**, **B**, **G** and **M** in Eq. (5) are given by Waas (1972), Kausel (1974) and Tassoulas (1981). For the CFABCs, element matrices in plane strain in Eq. (5a) can be written as (Lee and Tassoulas 2011)

$$\mathbf{A}^j = \frac{h_j}{4}\begin{bmatrix} \lambda_j+2\mu_j & 0 & \lambda_j+2\mu_j & 0 \\ 0 & \mu_j & 0 & \mu_j \\ \lambda_j+2\mu_j & 0 & \lambda_j+2\mu_j & 0 \\ 0 & \mu_j & 0 & \mu_j \end{bmatrix} \tag{6a}$$

$$\mathbf{B}^j = \frac{1}{2}\begin{bmatrix} 0 & -\lambda_j+\mu_j & 0 & \lambda_j+\mu_j \\ \lambda_j-\mu_j & 0 & \lambda_j+\mu_j & 0 \\ 0 & -\lambda_j-\mu_j & 0 & \lambda_j-\mu_j \\ -\lambda_j-\mu_j & 0 & -\lambda_j+\mu_j & 0 \end{bmatrix} \tag{6b}$$

$$\mathbf{G}^j = \frac{1}{h_j}\begin{bmatrix} \mu_j & 0 & -\mu_j & 0 \\ 0 & \lambda_j+2\mu_j & 0 & -(\lambda_j+2\mu_j) \\ -\mu_j & 0 & \mu_j & 0 \\ 0 & -(\lambda_j+2\mu_j) & 0 & \lambda_j+2\mu_j \end{bmatrix} \tag{6c}$$

$$\mathbf{M}^j = \frac{\rho_j h_j}{4}\begin{bmatrix} 1 & 0 & 1 & 0 \\ 0 & 1 & 0 & 1 \\ 1 & 0 & 1 & 0 \\ 0 & 1 & 0 & 1 \end{bmatrix} \tag{6d}$$

where the superscript and subscript j correspond to the j-th CFABC and h_j is depth of the j-th CFABC. Element matrices in antiplane shear in Eq. (5b) are given as follows

$$\mathbf{A}^j = \frac{h_j}{4}\begin{bmatrix} \mu_j & \mu_j \\ \mu_j & \mu_j \end{bmatrix} \tag{7a}$$

$$\mathbf{G}^j = \frac{1}{h_j}\begin{bmatrix} \mu_j & -\mu_j \\ -\mu_j & \mu_j \end{bmatrix} \tag{7b}$$

$$\mathbf{M}^j = \frac{\rho_j h_j}{4}\begin{bmatrix} 1 & 1 \\ 1 & 1 \end{bmatrix} \tag{7c}$$

Since the mid-point integration rule is used for the evaluation of the matrices in Eqs. (6) and (7), the matrices $\mathbf{A}^j$ and $\mathbf{M}^j$ are different from the ones for the ordinary layers. It has been shown (Lee and Tassoulas 2011) that, if the CFABCs are used, the Rayleigh wave mode of a half-space can be calculated almost exactly with only a shallow region of ordinary layers. Also, various characteristics of the calculated eigenvalues and eigenvectors have been examined by Lee and Tassoulas (2011).

Using the eigenvalues k and eigenvectors Δ obtained from Eq. (5), the consistent transmitting boundary is derived (Kausel 1974, Tassoulas 1981). The transmitting boundary is obtained by means of a synthesis of eigenmodes. For the far-field region of $r \geq r_0$, the dynamic stiffness $\mathbf{R}$ of the transmitting boundary for Fourier number m can be obtained as follows

$$\mathbf{R} = r_0\left\{\mathbf{A}\Psi\mathbf{K}^2 + (\mathbf{D} - \mathbf{E} + m\mathbf{N})\Phi\mathbf{K} - \left[\frac{m(m+1)}{2}\mathbf{L} + m\mathbf{Q}\right]\Psi\right\}\mathbf{Y}^{-1} \tag{8}$$

where $\mathbf{K}$ is the diagonal matrix of the eigenvalues. The modal matrices Ψ, Φ and $\mathbf{Y}$ are defined in Kausel (1974) and Tassoulas (1981). For the ordinary layers, the matrices $\mathbf{A}$, $\mathbf{D}$, $\mathbf{E}$, $\mathbf{N}$, $\mathbf{L}$ and $\mathbf{Q}$ in Eq. (8) are also given by Kausel (1974) and Tassoulas (1981). For the j-th CFABC, the element matrices are as follows

$$\mathbf{A}^j = \frac{h_j}{4}\begin{bmatrix} \lambda_j+2\mu_j & 0 & 0 & \lambda_j+2\mu_j & 0 & 0 \\ 0 & \mu_j & 0 & 0 & \mu_j & 0 \\ 0 & 0 & \mu_j & 0 & 0 & \mu_j \\ \lambda_j+2\mu_j & 0 & 0 & \lambda_j+2\mu_j & 0 & 0 \\ 0 & \mu_j & 0 & 0 & \mu_j & 0 \\ 0 & 0 & \mu_j & 0 & 0 & \mu_j \end{bmatrix} \tag{9a}$$

$$\mathbf{D}^j = \frac{1}{2}\begin{bmatrix} 0 & \lambda_j & 0 & 0 & -\lambda_j & 0 \\ -\mu_j & 0 & 0 & \mu_j & 0 & 0 \\ 0 & 0 & 0 & 0 & 0 & 0 \\ 0 & \lambda_j & 0 & 0 & -\lambda_j & 0 \\ -\mu_j & 0 & 0 & \mu_j & 0 & 0 \\ 0 & 0 & 0 & 0 & 0 & 0 \end{bmatrix} \tag{9b}$$

$$\mathbf{E}^j = \frac{1}{2}\frac{\mu_j h_j}{r_0}\begin{bmatrix} 1&0&0&1&0&0\\ 0&0&0&0&0&0\\ 0&0&1&0&0&1\\ 1&0&0&1&0&0\\ 0&0&0&0&0&0\\ 0&0&1&0&0&1 \end{bmatrix} \tag{9c}$$

$$\mathbf{N}^j = \frac{1}{4}\frac{\mu_j h_j}{r_0}\begin{bmatrix} 0&0&2&0&0&2\\ 0&1&0&0&1&0\\ 2&0&0&2&0&0\\ 0&0&2&0&0&2\\ 0&1&0&0&1&0\\ 2&0&0&2&0&0 \end{bmatrix} \tag{9d}$$

$$\mathbf{L}^j = \frac{\mu_j h_j}{r_0^2}\begin{bmatrix} 1&0&-1&1&0&-1\\ 0&0&0&0&0&0\\ -1&0&1&-1&0&1\\ 1&0&-1&1&0&-1\\ 0&0&0&0&0&0\\ -1&0&1&-1&0&1 \end{bmatrix} \tag{9e}$$

$$\mathbf{Q}^j = \frac{1}{2}\frac{\mu_j}{r_0}\begin{bmatrix} 0&0&0&0&0&0\\ 1&0&-1&1&0&-1\\ 0&0&0&0&0&0\\ 0&0&0&0&0&0\\ 1&0&-1&1&0&-1\\ 0&0&0&0&0&0 \end{bmatrix} \tag{9f}$$

Since the mid-point integration rule is also used for the evaluation of the matrices in Eq. (9), the matrices $\mathbf{A}^j$, $\mathbf{E}^j$, $\mathbf{N}^j$ and $\mathbf{L}^j$ are different from the ones for the ordinary layers. The far-field region of a layered half-space in Fig. 1 can be represented by the formulated consistent transmitting boundary combined with the CFABCs. The only undetermined parameter for the j-th CFABC is its thickness.

It has been shown (Lee and Tassoulas 2011) that the j-th CFABC with thickness of h_j is a perfect absorber for waves with a vertical wavenumber $l = l_j = -2i/h_j$ (Guddati 2006). However, it is not a perfect absorber for waves with a given horizontal or apparent wavenumber k. This is because there are two kinds of waves for a wavenumber k: P and S waves. The P and S waves with an identical wavenumber k have different vertical wavenumbers $l = l_p = \sqrt{\omega^2/C_p^2 - k^2}$ and $l = l_s = \sqrt{\omega^2/C_s^2 - k^2}$, respectively, where C_p and C_s are the wave speeds for the P and S waves, respectively. Thus, the single CFABC layer with thickness h_j is not a perfect absorber for waves with a horizontal wavenumber k. In order to be a perfect absorber for waves with a wavenumber k in a layered half-

space, it was proposed that layers of the CFABC be used in the form of 2-layers (Lee and Tassoulas 2011). One layer is designed to absorb the P wave and the other the S wave. Each of the 2 layers has thicknesses of $h_p = -2i/l_p$ and $h_s = -2i/l_s$, respectively. The perfect absorption of the 2-layer can be proved easily. Also, a method for determination of thicknesses of the 2-layer has been proposed for evanescent waves as well as propagating waves (Lee and Tassoulas 2011). The terms 'propagating' and 'evanescent' in this context refer to characteristics of waves in the vertical direction of layering. The propagating waves in the vertical direction have a real vertical wavenumber l and the evanescent ones an imaginary wavenumber l. Therefore, CFABC layers must have imaginary and real thicknesses for the propagating and evanescent waves, respectively. For vertically-propagating P and S waves with a horizontal wavenumber k, the thicknesses of the 2-layer are

$$h_P = -\frac{2iC_P}{\omega\cos\theta_P} \tag{10a}$$

$$h_S = -\frac{2iC_S}{\omega\cos\theta_S} \tag{10b}$$

$$\frac{\sin\theta_P}{\sin\theta_S} = \frac{C_P}{C_S} \tag{10c}$$

where θ_P and θ_S are incidence angles with respect to the z axis. For an evanescent Rayleigh surface wave with velocity C_R, the thicknesses of the CFABC 2-layer can be written as

$$h_P = \frac{2C_P}{\omega\sqrt{\alpha_P^2 - 1}} \tag{11a}$$

$$h_S = \frac{2C_S}{\omega\sqrt{\alpha_S^2 - 1}} \tag{11b}$$

$$\frac{\alpha_P}{\alpha_S} = \frac{C_P}{C_S} \tag{11c}$$

where $\alpha_P = C_P/C_R > 1$ and $\alpha_S = C_S/C_R > 1$. Using the thicknesses of Eqs. (10) and (11), the element matrices in Eqs. (6), (7) and (9) are calculated.

3. Effects of obliquely incident seismic waves

A layered half-space is modeled by conventional finite elements in the near-field region and the consistent transmitting boundary derived in Section 2 in the far-field region. In this section, the effects of obliquely incident seismic waves in a layered half-space will be taken into account in the formulation of the transmitting boundary.

Consider a free field in the layered half-space (Fig. 2(a)) subjected to obliquely incident seismic waves, with an apparent wave velocity of C_{app} and wavenumber of $k_{app} = \omega/C_{app}$ on the free-field surface. For vertically incident wave, $C_{app} = \infty$ and $k_{app} = 0$. Assumed are the time- and x-harmonic waves with $e^{i(\omega t - k_{app}x)}$ term. The incident waves are applied at the base at $z = z_{N+1}$ and result in free-field motions in the half-space. Applying base motions at $z = z_{N+1}$ and solving the wave propagation

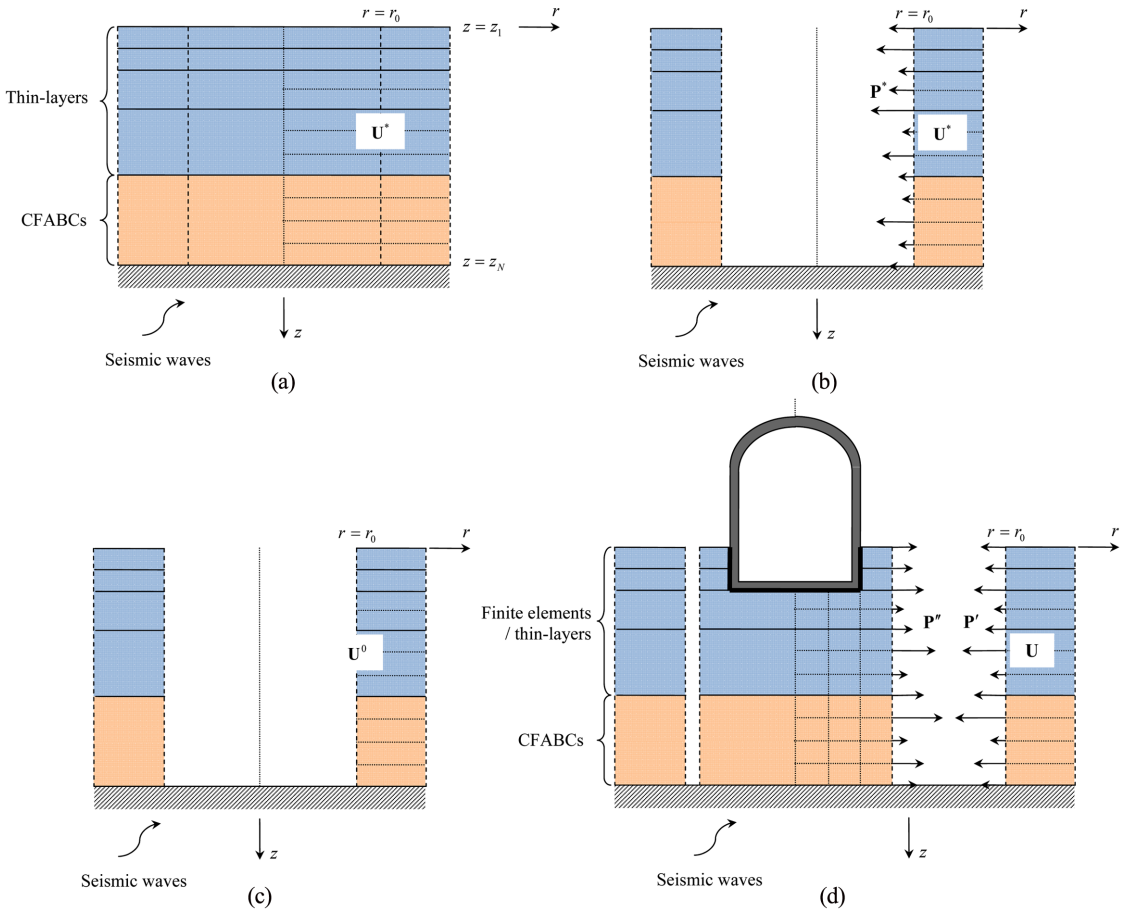

Fig. 2 Effects of obliquely incident seismic waves: (a) free field, (b) removal of the cylindrical region of $r \le r_0$, (c) cylindrical region of $r \ge r_0$ with free boundary condition and (d) soil-structure interaction system

problems of Eqs. (12) and (13) with free surface specified at $z = z_1$, the free-field motions $\mathbf{U}^*_{P-SV}$ and $\mathbf{U}^*_{SH}$ are obtained

$$[k^2_{app}\mathbf{A} + ik_{app}\mathbf{B} + \mathbf{G} - \omega^2\mathbf{M}]\mathbf{U}^*_{P-SV} = \mathbf{0} \quad \text{for } P \text{ and } SV \text{ waves} \tag{12a}$$

$$\mathbf{U}^*_{P-SV} = \langle U^*_x(z_1)\ U^*_z(z_1)\ \cdots\ U^*_x(z_{N+1})\ U^*_z(z_{N+1})\rangle^T \tag{12b}$$

$$[k^2_{app}\mathbf{A} + \mathbf{G} - \omega^2\mathbf{M}]\mathbf{U}^*_{SH} = \mathbf{0} \text{ for an } SH \text{ wave} \tag{13a}$$

$$\mathbf{U}^*_{SH} = \langle U^*_y(z_1)\ \cdots\ U^*_y(z_{N+1})\rangle^T \tag{13b}$$

where the matrices **A**, **B**, **G** and **M** are the same as the ones used in Eq. (5). The free-field motions of Eqs. (12) and (13) can be expressed in the cylindrical coordinate systems as follows (Kausel 1974)

for symmetric motion

$$u_r^*(r,\theta,z) = \bar{u}_r^*(r,z)\cos m\theta = \frac{2}{1+\delta_{m0}} U_x^*(z) \frac{i^{m+1}}{k_{app}} \frac{dJ_m(-k_{app}r)}{dr} \cos m\theta \tag{14a}$$

$$u_z^*(r,\theta,z) = \bar{u}_z^*(r,z)\cos m\theta = \frac{2}{1+\delta_{m0}} U_z^*(z) i^m J_m(-k_{app}r)\cos m\theta \tag{14b}$$

$$u_\theta^*(r,\theta,z) = -\bar{u}_\theta^*(r,z)\sin m\theta = -\frac{2}{1+\delta_{m0}} U_x^*(z) \frac{mi^{m+1}}{k_{app}r} J_m(-k_{app}r)\sin m\theta \tag{14c}$$

for anti-symmetric motion

$$u_r^*(r,\theta,z) = \bar{u}_r^*(r,z)\sin m\theta = \frac{2}{1+\delta_{m0}} U_y^*(z) \frac{mi^{m+1}}{k_{app}r} J_m(-k_{app}r)\sin m\theta \tag{15a}$$

$$u_z^*(r,\theta,z) = \bar{u}_z^*(r,z)\sin m\theta = 0 \tag{15b}$$

$$u_\theta^*(r,\theta,z) = \bar{u}_\theta^*(r,z)\cos m\theta = \frac{2}{1+\delta_{m0}} U_y^*(z) \frac{i^{m+1}}{k_{app}} \frac{dJ_m(-k_{app}r)}{dr} \cos m\theta \tag{15c}$$

where δ_{m0} is the Kronecker delta and $J_m(-k_{app}r)$ the Bessel function of order m. From Eqs. (14) and (15), the Fourier amplitude of nodal displacement vector $\mathbf{U}^*$ at the cylindrical boundary of $r = r_0$ in the free field can be obtained

for symmetric motion

$$\begin{cases} U_{3j-2}^* = \bar{u}_r^*(r_0,z_j) = \dfrac{2}{1+\delta_{m0}} U_x^*(z_j) \dfrac{i^{m+1}}{k_{app}} \dfrac{dJ_m(-k_{app}r)}{dr}\Big|_{r=r_0} \\ U_{3j-1}^* = \bar{u}_z^*(r_0,z_j) = \dfrac{2}{1+\delta_{m0}} U_z^*(z_j) i^m J_m(-k_{app}r_0) \qquad \text{for } 1 \le j \le N \\ U_{3j}^* = \bar{u}_\theta^*(r_0,z_j) = \dfrac{2}{1+\delta_{m0}} U_x^*(z_j) \dfrac{mi^{m+1}}{k_{app}r_0} J_m(-k_{app}r_0) \end{cases} \tag{16a}$$

for anti-symmetric motion

$$\begin{cases} U_{3j-2}^* = \bar{u}_r^*(r_0,z_j) = \dfrac{2}{1+\delta_{m0}} U_y^*(z_j) \dfrac{mi^{m+1}}{k_{app}r_0} J_m(-k_{app}r_0) \\ U_{3j-1}^* = \bar{u}_z^*(r_0,z_j) = 0 \qquad \text{for } 1 \le j \le N \\ U_{3j}^* = \bar{u}_\theta^*(r_0,z_j) = \dfrac{2}{1+\delta_{m0}} U_y^*(z_j) \dfrac{i^{m+1}}{k_{app}} \dfrac{dJ_m(-k_{app}r)}{dr}\Big|_{r=r_0} \end{cases} \tag{16b}$$

If the cylindrical region of $r \le r_0$ is removed from the free-field, consistent nodal forces must be applied at the cylindrical boundary of $r = r_0$ to preserve equilibrium (Fig. 2(b)). The vector of consistent nodal forces, $\mathbf{P}^*$, can be calculated as follows

$$\mathbf{P}^* = -r_0 \int \mathbf{N}^T(z) \begin{Bmatrix} \bar{\sigma}_r^*(r_0, z) \\ \bar{\tau}_{rz}^*(r_0, z) \\ \bar{\tau}_{r\theta}^*(r_0, z) \end{Bmatrix} dz = r_0 \left\{ k_{app}\mathbf{A}\boldsymbol{\Psi}^* + [\mathbf{D} - \mathbf{E} + m\mathbf{N}]\boldsymbol{\Phi}^* - \frac{1}{k_{app}} \left[\frac{m(m+1)}{2}\mathbf{L} + m\mathbf{Q} \right] \boldsymbol{\Psi}^* \right\} \quad (17)$$

where $\mathbf{N}(z)$ is the shape-function matrix on the boundary and $\bar{\sigma}_r^*(r, z)$, $\bar{\tau}_{rz}^*(r, z)$ and $\bar{\tau}_{r\theta}^*(r, z)$ are Fourier amplitudes of stress components of the free-field calculated from the free-field motions of Eqs. (14) and (15). The matrices **A**, **D**, **E**, **N**, **L** and **Q** in Eq. (17) are the same as the ones in Eq. (8) and the matrices $\boldsymbol{\Psi}^*$ and $\boldsymbol{\Phi}^*$ are given as follows

for symmetric motion

$$\begin{cases} \Psi_{3j-2}^* = \dfrac{2}{1+\delta_{m0}} i^{m+1} U_x^*(z_j) J_m(-k_{app} r_0) \\ \Psi_{3j-1}^* = \dfrac{2}{1+\delta_{m0}} i^{m} U_z^*(z_j) J_{m-1}(-k_{app} r_0) \\ \Psi_{3j}^* = 0 \end{cases} \quad \text{for } 1 \le j \le N \quad (18a)$$

$$\begin{cases} \Phi_{3j-2}^* = \dfrac{2}{1+\delta_{m0}} i^{m+1} U_x^*(z_j) J_{m-1}(-k_{app} r_0) \\ \Phi_{3j-1}^* = \dfrac{2}{1+\delta_{m0}} i^{m} U_z^*(z_j) J_m(-k_{app} r_0) \\ \Phi_{3j}^* = 0 \end{cases} \quad \text{for } 1 \le j \le N \quad (18b)$$

for anti-symmetric motion

$$\begin{cases} \Psi_{3j-2}^* = 0 \\ \Psi_{3j-1}^* = 0 \\ \Psi_{3j}^* = \dfrac{2}{1+\delta_{m0}} i^{m+1} U_y^*(z_j) J_m(-k_{app} r_0) \end{cases} \quad \text{for } 1 \le j \le N \quad (19a)$$

$$\begin{cases} \Phi_{3j-2}^* = 0 \\ \Phi_{3j-1}^* = 0 \\ \Phi_{3j}^* = \dfrac{2}{1+\delta_{m0}} i^{m+1} U_y^*(z_j) J_{m-1}(-k_{app} r_0) \end{cases} \quad \text{for } 1 \le j \le N \quad (19b)$$

The motion $\mathbf{U}^0$ of the cylindrical far-field region of $r \geq r_0$ with free boundary at $r = r_0$ (Fig. 2(c)) can be obtained by application of forces opposite to $\mathbf{P}^*$ on the boundary as follows

$$\mathbf{U}^0 = \mathbf{U}^* - \mathbf{R}^{-1}\mathbf{P}^* \tag{20}$$

If the structure and near-field region are included, the motion $\mathbf{U}$ of the boundary at $r = r_0$ is no longer the motion $\mathbf{U}^0$ (Fig. 2(d)). There are also interaction forces $\mathbf{P}'$ and $\mathbf{P}''$ applied to the far- and near-field regions, respectively. Since the motion $\mathbf{U}^0$ is obtained from the free boundary condition on the boundary of $r = r_0$, the vector $\mathbf{P}'$ is given as follows

$$\mathbf{P}' = \mathbf{R}(\mathbf{U} - \mathbf{U}^0) = \mathbf{R}\mathbf{U} - \mathbf{R}\mathbf{U}^* + \mathbf{P}^* \tag{21}$$

where Eq. (20) has been used. The equation of motion of the structure and near-field region can be written as

$$(-\omega^2\mathbf{M}_{NF} + i\omega\mathbf{C}_{NF} + \mathbf{K}_{NF})\mathbf{U} = \mathbf{P}'' \tag{22}$$

where $\mathbf{M}_{NF}$, $\mathbf{C}_{NF}$ and $\mathbf{K}_{NF}$ are mass, damping and stiffness matrices, respectively. In Eq. (22), the number of entries in $\mathbf{P}''$ is increased with as many zeros as necessary to match the dimensions of $\mathbf{M}_{NF}$, $\mathbf{C}_{NF}$ and $\mathbf{K}_{NF}$. Since the interaction forces are opposite to each other, i.e., $\mathbf{P}' + \mathbf{P}'' = \mathbf{0}$, Eqs. (21) and (22) can be combined by increasing the numbers of rows and columns in the vectors and matrices of Eq. (21)

$$(-\omega^2\mathbf{M}_{NF} + i\omega\mathbf{C}_{NF} + \mathbf{K}_{NF} + \mathbf{R})\mathbf{U} = \mathbf{R}\mathbf{U}^* - \mathbf{P}^* \tag{23}$$

Eq. (23) is the final equation of motion for the soil-structure interaction system subjected to the obliquely incident seismic waves.

4. Applications

Using the numerical method presented in the previous sections, impedance (and compliance) functions and input motions of rigid circular foundations on the surface of or embedded in a homogeneous half-space will be computed. The impedance and compliance functions for rigid circular and cylindrical foundations can be written as

$$\begin{Bmatrix} M_z \\ F_z \\ F_x \\ M_y \\ F_y \\ M_x \end{Bmatrix} = \begin{bmatrix} K_{TT} & & & & & \\ & K_{VV} & & & & \\ & & K_{HH} & K_{HR} & & \\ & & K_{RH} & K_{RR} & & \\ & & & & K_{HH} & -K_{HR} \\ & & & & -K_{RH} & K_{RR} \end{bmatrix} \begin{Bmatrix} \phi_z \\ \Delta_z \\ \Delta_x \\ \phi_y \\ \Delta_y \\ \phi_x \end{Bmatrix} \tag{24a}$$

$$\begin{Bmatrix} \phi_z \\ \Delta_z \\ \Delta_x \\ \phi_y \\ \Delta_y \\ \phi_x \end{Bmatrix} = \begin{bmatrix} C_{TT} & & & & & \\ & C_{VV} & & & & \\ & & C_{HH} & C_{HR} & & \\ & & C_{RH} & C_{RR} & & \\ & & & & C_{HH} & -C_{HR} \\ & & & & -C_{RH} & C_{RR} \end{bmatrix} \begin{Bmatrix} M_z \\ F_z \\ F_x \\ M_y \\ F_y \\ M_x \end{Bmatrix} \tag{24b}$$

It should be noted that $K_{HR} = K_{RH}$ and $C_{HR} = C_{RH}$ in Eq. (24). It is usual to introduce stiffness and damping coefficients for the impedance functions. The stiffness and damping coefficients are defined as follows

$$K_{TT} = \mu^* R^3 (k_{TT} + i a_0 c_{TT}) \tag{25a}$$

$$K_{VV} = \mu^* R (k_{VV} + i a_0 c_{VV}) \tag{25b}$$

$$K_{HH} = \mu^* R (k_{HH} + i a_0 c_{HH}) \tag{25c}$$

$$K_{RR} = \mu^* R^3 (k_{RR} + i a_0 c_{RR}) \tag{25d}$$

$$K_{HR} = \mu^* R^2 (k_{HR} + i a_0 c_{HR}) \tag{25e}$$

where $\mu^* = \mu(1 + 2i\beta_s)$ is the complex shear modulus with hysteretic damping ratio β_s, R the foundation radius and $a_0 = \omega R / C_s$ a dimensionless frequency. The input motions for the rigid circular and cylindrical foundations are defined as follows

$$\begin{Bmatrix} R\phi_z^* \\ \Delta_z^* \\ \Delta_x^* \\ R\phi_y^* \\ \Delta_y^* \\ R\phi_x^* \end{Bmatrix} = \begin{bmatrix} & & R_{zy} \\ S_{zx} & S_{zz} & \\ S_{xx} & S_{xz} & \\ R_{yx} & R_{yz} & \\ & & S_{yy} \\ & & R_{xy} \end{bmatrix} \begin{Bmatrix} U_x^*(z_1) \\ U_z^*(z_1) \\ U_y^*(z_1) \end{Bmatrix} \tag{26}$$

For a surface circular foundation subjected to vertically incident waves, the transfer functions in Eq. (26) are: $S_{xx} = S_{yy} = 1$, $S_{zz} = 1$, $S_{xz} = S_{zx} = 0$, $R_{yx} = -R_{xy} = 0$ and $R_{yz} = -R_{zy} = 0$. For a embedded cylindrical foundation subjected to vertically incident waves, $S_{xx} = S_{yy}$, $S_{xz} = S_{zx} = 0$, $R_{yx} = -R_{zy}$ and $R_{yz} = -R_{zy} = 0$. For obliquely incident waves, all transfer functions must be calculated.

4.1 Surface circular foundation

Compliance functions and input motions of a rigid circular foundation on the surface of a homogeneous half-space in Fig. 3(a) will be calculated first. Poisson's ratio ν of the half-space is 1/3 ($C_p = 2C_s$). A very small amount of hysteretic damping ($\beta_s = 0.005$) is included for the numerical calculations. The near-field region is discretized using conventional finite elements. On the other hand, the consistent transmitting boundary is placed at $r = R$ for a representation of the far field, $r \geq R$. Both regions are truncated at the depth of $H = 4R$ and two 2-layers of the CFABCs are applied at the bottom to represent the effects of the half-space in the vertical direction. One of the 2-layers is for an evanescent wave and the other for a vertically propagating wave. Since the velocity C_R of the Rayleigh surface wave for the half-space is $0.9325C_s$, the parameters α_P and α_S for the evanescent wave in Eq. (11) are 2.1448 and 1.0724, respectively. For the vertically propagating wave, only a vertically-incident wave is considered and the parameters θ_P and θ_S in Eq. (10) are 0. The finite-element mesh is shown in Fig. 3(b). It should be noted that the size of the finite elements and layer thickness in the transmitting boundaries is selected consistently with the shear-wave speed of the half-space and the maximum frequency of interest. The longest side is about 1/6 of the minimum shear-wave length for the considered range of frequencies.

The compliance functions C_{TT}, C_{VV}, C_{HH}, C_{RR} and C_{HR} are calculated and normalized by the static

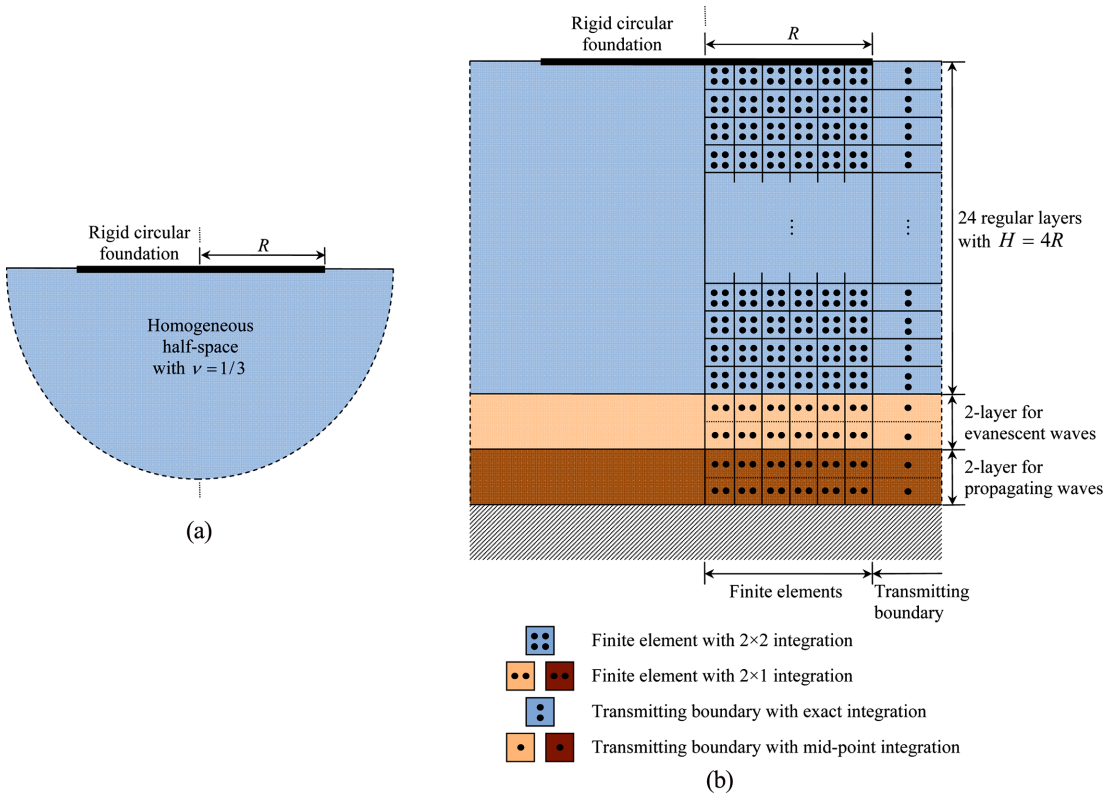

Fig. 3 Rigid circular foundation on the surface of a homogeneous half-space: (a) schematic view of problem and (b) finite-element mesh

compliances equal to $3/16\mu R^3$, $(1-\nu)/4\mu R$, $(2-\nu)/8\mu R$, $3(1-\nu)/8\mu R^3$, and $3(1-2\nu)/16\pi\mu R^2$ for C_{TT}, C_{VV}, C_{HH}, C_{RR} and C_{HR}, respectively. In Fig. 4, the compliance functions are shown to compare favorably with those obtained from impedance functions reported by Luco and Mita (1987). Discrepancies between the present numerical results and the analytical ones of Luco and Mita (1987) are, to a great extent, typical of the discretization errors inherent in finite-element computations. Mesh refinement leads to reduction of the relatively "stiff" response that is a

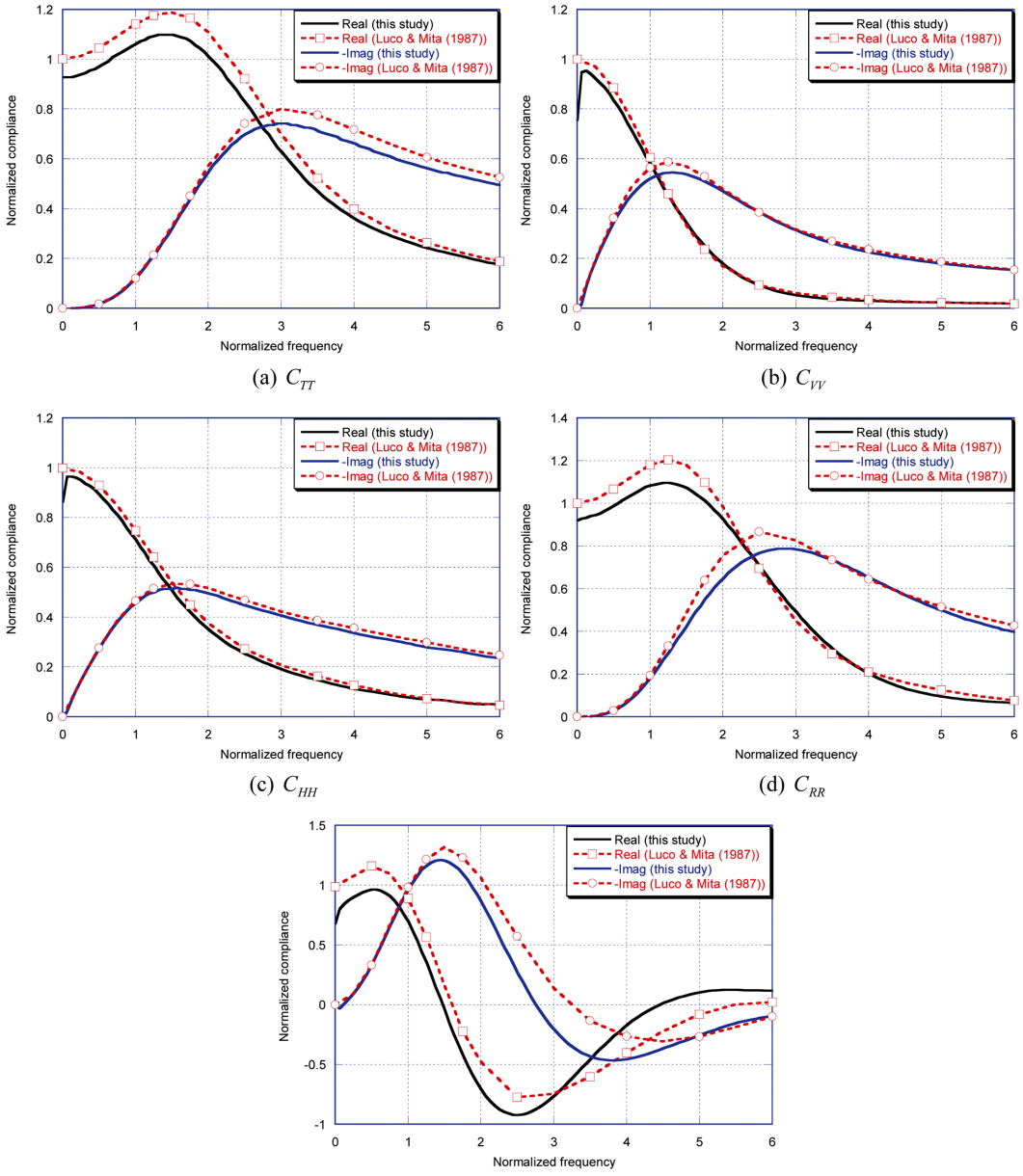

(a) C_{TT} (b) C_{VV}

(c) C_{HH} (d) C_{RR}

(e) C_{HR}

Fig. 4 Compliance functions of a surface circular foundation

consequence of discretization. Differences in the coupling compliance (C_{HR}) are largely due to the relaxed contact conditions adopted in the analytical work by Luco and Mita (1987). Finally, deviations of the computational results from the analytical ones in the very-low frequency range are a consequence of the approximation that underlies the CFABCs. These very-low frequency results will be examined further and improved using extrapolation methods below.

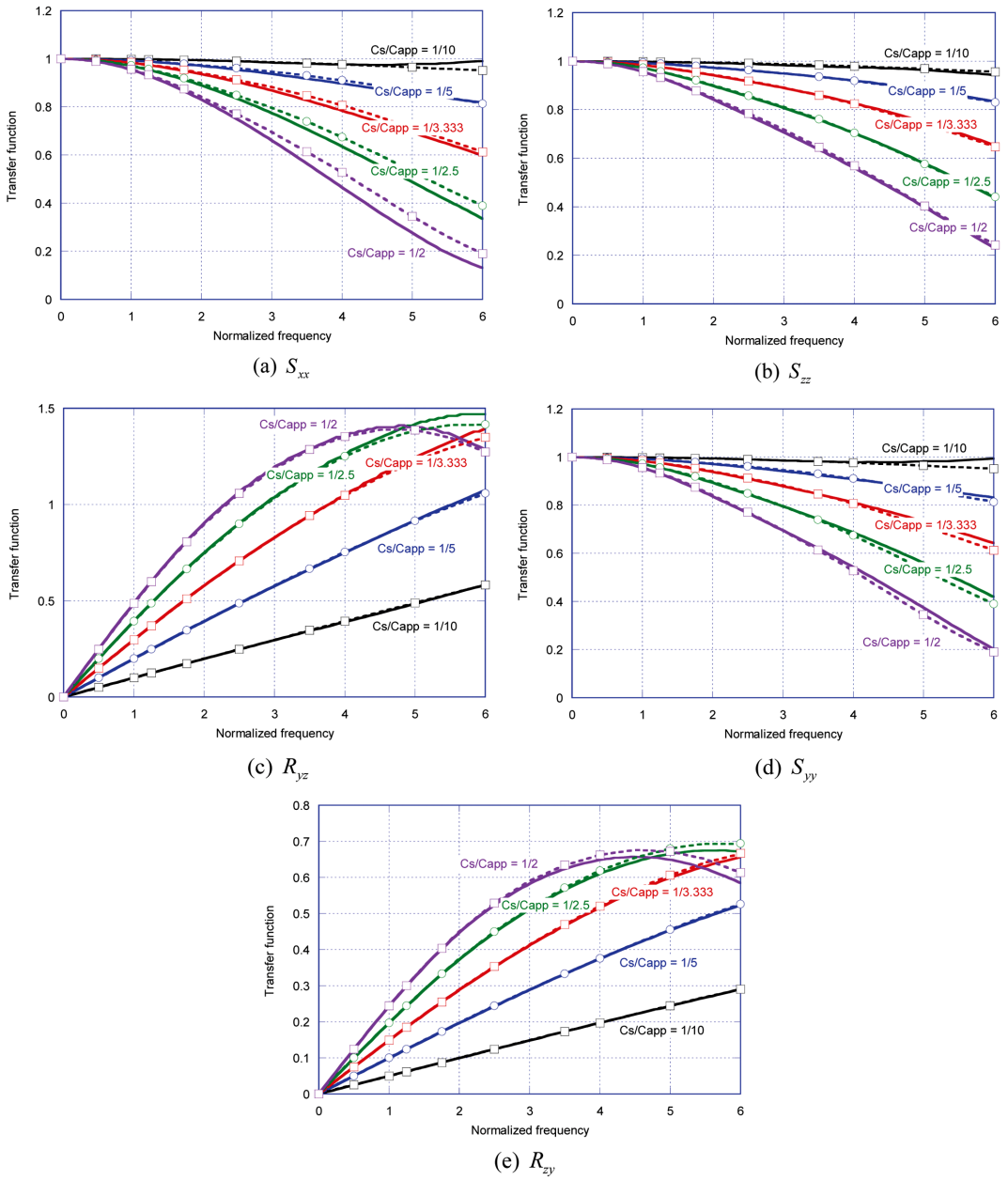

Fig. 5 Amplitudes of transfer functions of a surface circular foundation (solid lines for this study and dashed lines for Luco and Mita (1987))

Also, the transfer functions S_{xx}, S_{zz}, R_{yz}, S_{yy} and R_{zy} are calculated for $C_s/C_{app} = 1/10$, 1/5, 1/3.333, 1/2.5 and 1/2. In Fig. 5, the transfer functions are compared with Luco and Mita's results (1987). Because of the relaxed contact conditions, these five transfer functions are the nonvanishing ones in Luco and Mita's results. If the exact (rough) contact conditions are used, other transfer functions in Eq. (26) are also nonzero. It can be seen in Fig. 5 that the numerical method presented in the previous sections produces accurate results.

4.2 Embedded cylindrical foundation

Compliance functions and input motions of a rigid cylindrical foundation embedded in a homogeneous half-space in Fig. 6(a) are examined next. Poisson's ratio ν of the half-space is 1/4 ($C_P = \sqrt{3}\, C_S$). The discretization of the near and far fields shown in Fig. 6(b) is similar to that of the previous application, except for the excavated region of soil for the embedment of foundation and the parameters α_P and α_S in Eq. (11). In the cases examined herein, the depth of embedment E is set equal to 0 (a surface circular foundation), $0.5R$, $1.0R$ and $2.0R$. Since the velocity C_R of the Rayleigh surface wave for the half-space is $0.919C_S$, the parameters α_P and α_S for the evanescent wave in Eq. (11) are 1.884 and 1.088, respectively.

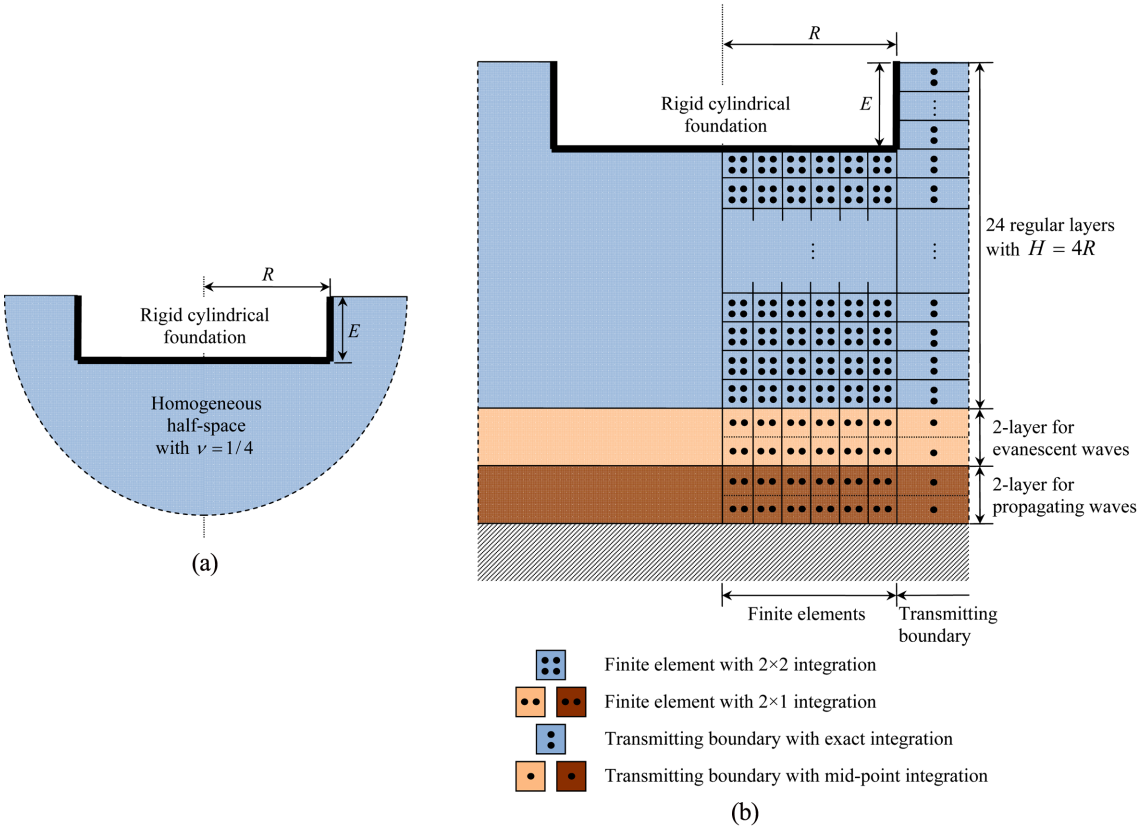

Fig. 6 Rigid cylindrical foundation embedded in a homogeneous half-space: (a) schematic view of problem and (b) finite-element mesh

The computed stiffness and damping coefficients are compared in Fig. 7 with those from Day's study (1977). The transfer functions $S_{xx} = S_{yy}$ and $R_{yx} = -R_{xy}$ for a vertically incident S wave are calculated. Also, the transfer functions S_{yy} and R_{zy} for a horizontally incident SH wave are obtained. The calculated transfer functions are compared with those of Day (1977) in Figs. 8 and 9. It is

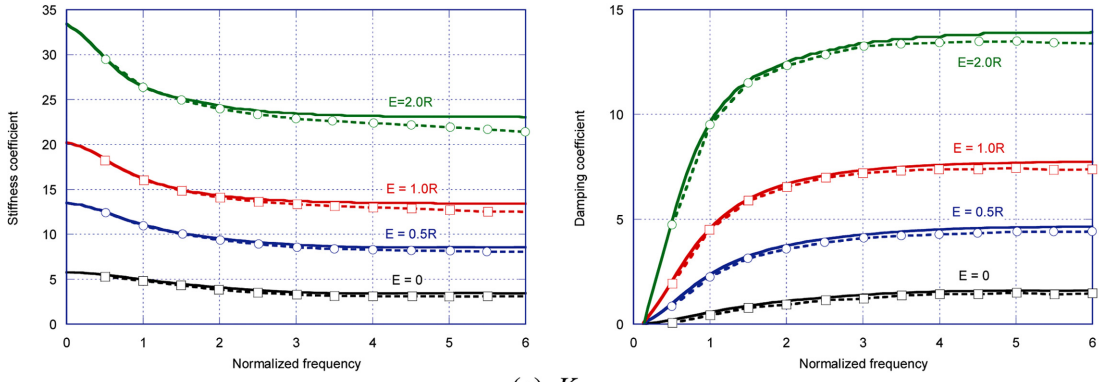

(a) K_{TT}

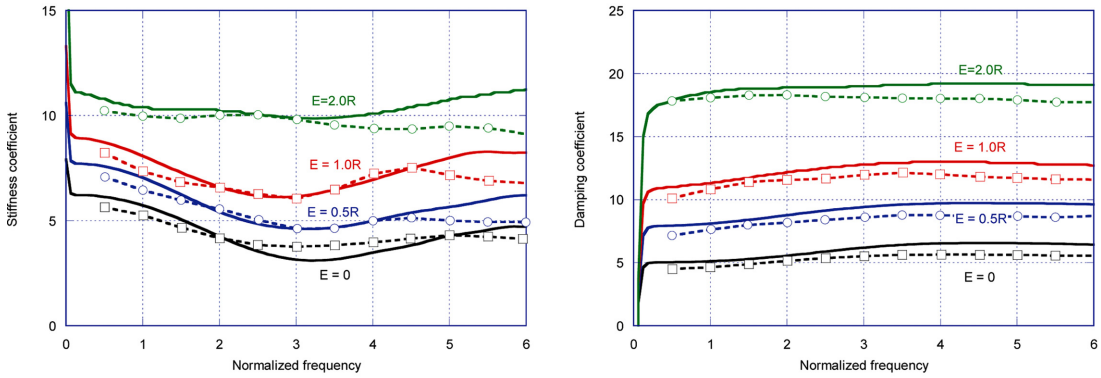

(b) K_{VV}

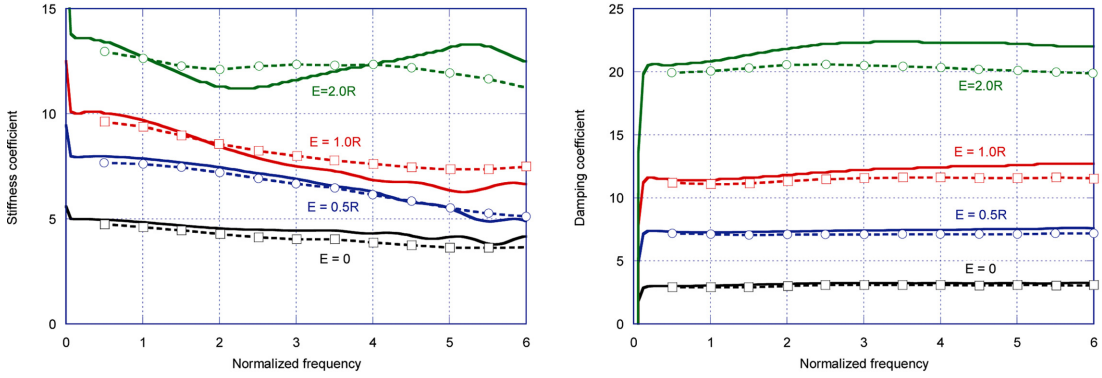

(c) K_{HH}

Fig. 7 Impedance functions of an embedded cylindrical foundation (solid lines for this study and dashed lines for Day (1977))

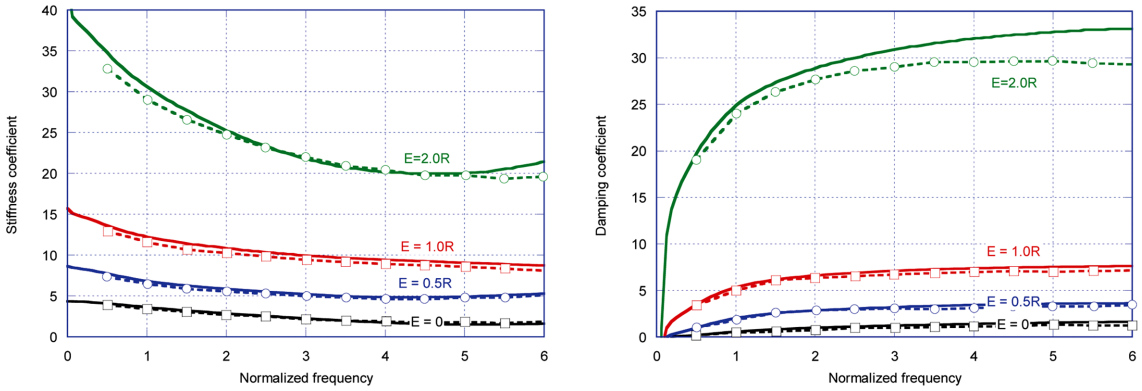

(d) K_{RR}

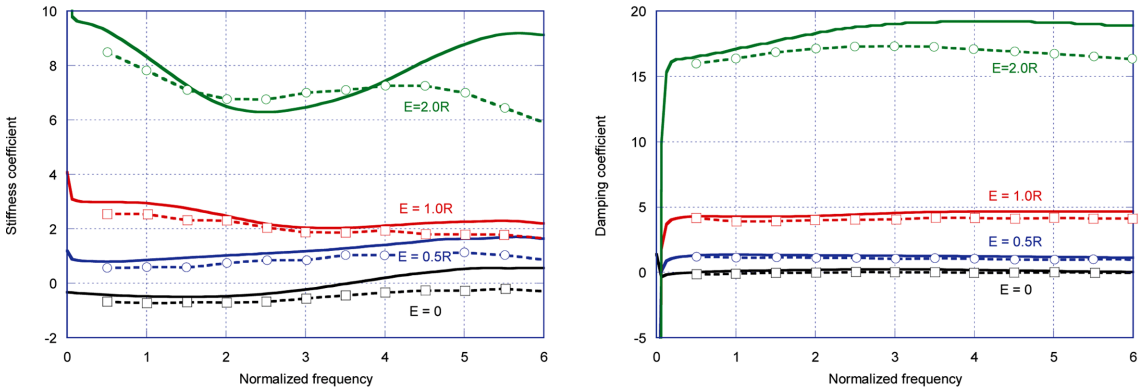

(e) K_{HR}

Fig. 7 Continued

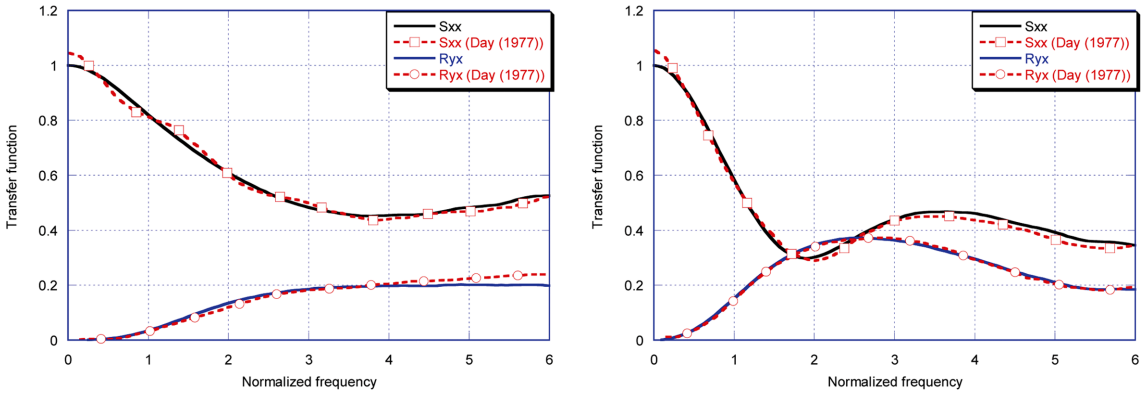

(a) $E = 0.5R$ (b) $E = 1.0R$

Fig. 8 Amplitudes of transfer functions of an embedded cylindrical foundation subjected to a vertically incident *S* wave

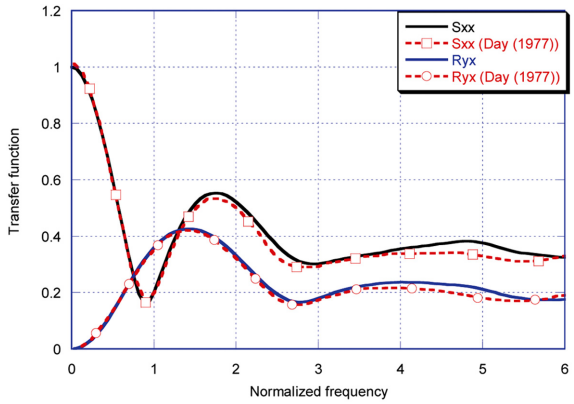

(c) $E = 2.0R$

Fig. 8 Continued

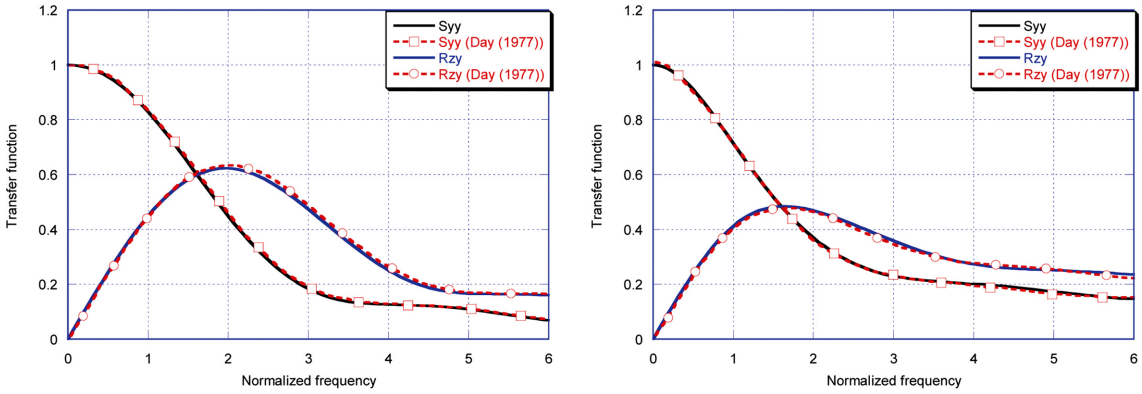

(a) $E = 0$ (b) $E = 0.5R$

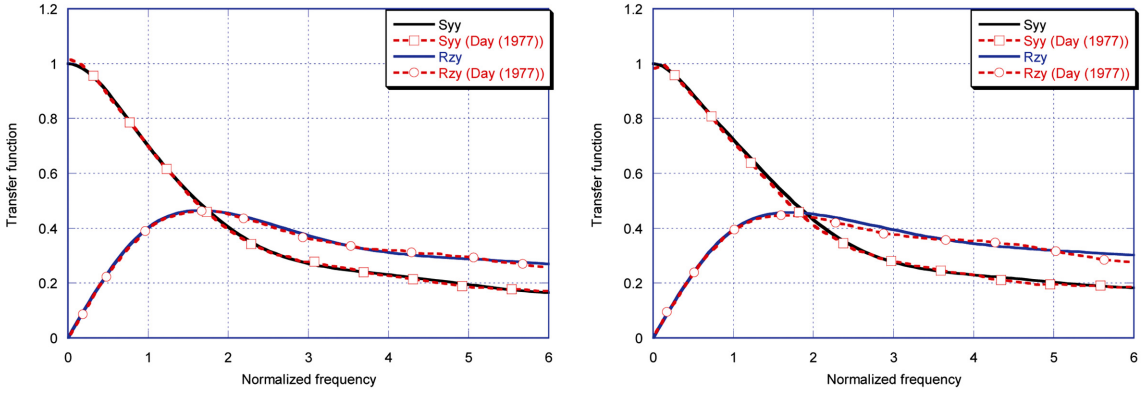

(c) $E = 1.0R$ (d) $E = 2.0R$

Fig. 9 Amplitudes of transfer functions of an embedded cylindrical foundation subjected to a horizontally incident *SH* wave

observed that the numerical method presented in this paper leads to good results. However, the stiffness and damping coefficients deviate from the available estimates in the very-low-frequency range.

Overall, the above applications indicate that the present numerical method performs well as a tool for dynamic analysis of foundations in a half-space.

4.3 Extrapolation into the very-low-frequency range and the static condition

The differences noted above between the numerical results and other available estimates in the very-low-frequency range are due to intrinsic characteristics of the CFABCs. Specifically, the CFABC layers have very large thicknesses in the very-low-frequency range (see Eqs. 10 and 11). The very large thicknesses lead to deterioration of the results in this range. Also, it can be deduced from Eqs. (10) and (11) that the thicknesses of the CFABCs become infinite for the static condition. Therefore, the numerical method presented in the previous sections cannot be applied for static analysis directly. To overcome these difficulties, two extrapolation methods for the very-low-frequency range and static condition are proposed.

Expressions for asymptotic behaviors at low frequency have been derived for the surface circular foundation and are given in the Appendix (Robertson 1966, Thomas 1968, Galdwell 1968). The first extrapolation method is based on these expressions. Real and imaginary parts of the extrapolated compliance and impedance functions are assumed proportional to those of the asymptotic expressions

$$C^e_{TT} = A_{TT,R}\left(1+\frac{1}{5}a_0^2-\frac{34}{525}a_0^4\right)+iA_{TT,I}\left(-\frac{4}{9\pi}a_0^3+\frac{16}{225\pi}a_0^5\right) \quad \text{for } a_0 \le a_0^e \tag{27a}$$

$$C^e_{VV} = A_{VV,R}\left(1-\frac{2I_2}{3\pi}a_0^2-\frac{-120\pi^3 I_4+204\pi^2 I_1 I_3+19\pi^2 I_2^2+720 I_1^4-960\pi I_1^2 I_2}{180\pi^4}a_0^4\right) + iA_{VV,I}\left(-\frac{I_1}{\pi}a_0-\frac{\pi^2 I_3-8\pi I_1 I_2+6I_1^3}{3\pi^3}a_0^3\right) \quad \text{for } a_0 \le a_0^e \tag{27b}$$

$$C^e_{HH} = A_{HH,R}\left(1-\frac{1}{3}B_2 a_0^2\right)+iA_{HH,I}\left(-B_1 a_0+\frac{2}{3}B_3 a_0^3\right) \quad \text{for } a_0 \le a_0^e \tag{27c}$$

$$C^e_{RR} = A_{RR,R}\left(1+\frac{2I_2}{5\pi}a_0^2-\frac{90\pi I_4+I_2^2}{525\pi^2}a_0^4\right)+iA_{RR,I}\left(-\frac{I_3}{3\pi}a_0^3+\frac{I_5}{15\pi}a_0^5\right) \quad \text{for } a_0 \le a_0^e \tag{27d}$$

The coefficients are determined so that the extrapolated functions match the computed results at a user-defined frequency. For example, using the numerical method presented in the previous sections, the compliance functions C_{TT}, C_{VV}, C_{HH} and C_{RR} are first calculated for $a_0 \ge a_0^e$. The coefficients $A_{TT,R}$, $A_{TT,I}$, $A_{VV,R}$, $A_{VV,I}$, $A_{HH,R}$, $A_{HH,I}$, $A_{RR,R}$ and $A_{RR,I}$ are then determined so that $C^e_{TT} = C_{TT}$, $C^e_{VV} = C_{VV}$, $C^e_{HH} = C_{HH}$ and $C^e_{RR} = C_{RR}$ at $a_0 = a_0^e$. The method can be applied to any foundation stiffness with known asymptotic behavior.

Expressions for asymptotic behaviors at low frequency are not available for arbitrary surface or cylindrical foundations. Therefore, a second, more general extrapolation method is proposed. The extrapolated compliance and impedance functions have similar forms to the asymptotic expressions given in the Appendix (but with different coefficients)

$$C_{TT}^{e} = (A_{TT,0} + A_{TT,2}a_0^2) + i(A_{TT,3}a_0^3 + A_{TT,5}a_0^5) \quad \text{for } a_0 \le a_0^e \tag{28a}$$

$$C_{VV}^{e} = (A_{VV,0} + A_{VV,2}a_0^2) + i(A_{VV,1}a_0 + A_{VV,3}a_0^3) \quad \text{for } a_0 \le a_0^e \tag{28b}$$

$$C_{HH}^{e} = (A_{HH,0} + A_{HH,2}a_0^2) + i(A_{HH,1}a_0 + A_{HH,3}a_0^3) \quad \text{for } a_0 \le a_0^e \tag{28c}$$

$$C_{RR}^{e} = (A_{RR,0} + A_{RR,2}a_0^2) + i(A_{RR,3}a_0^3 + A_{RR,5}a_0^5) \quad \text{for } a_0 \le a_0^e \tag{28d}$$

$$C_{HR}^{e} = (A_{HR,0} + A_{HR,2}a_0^2) + i(A_{HR,1}a_0 + A_{HR,3}a_0^3) \quad \text{for } a_0 \le a_0^e \tag{28e}$$

The coefficients are determined so that the extrapolated functions and their derivatives match the calculated numerical results at a user-defined frequency. For example, using the numerical method presented in the previous sections, the compliance function C_{TT} for $a_0 \ge a_0^e$ is computed. The

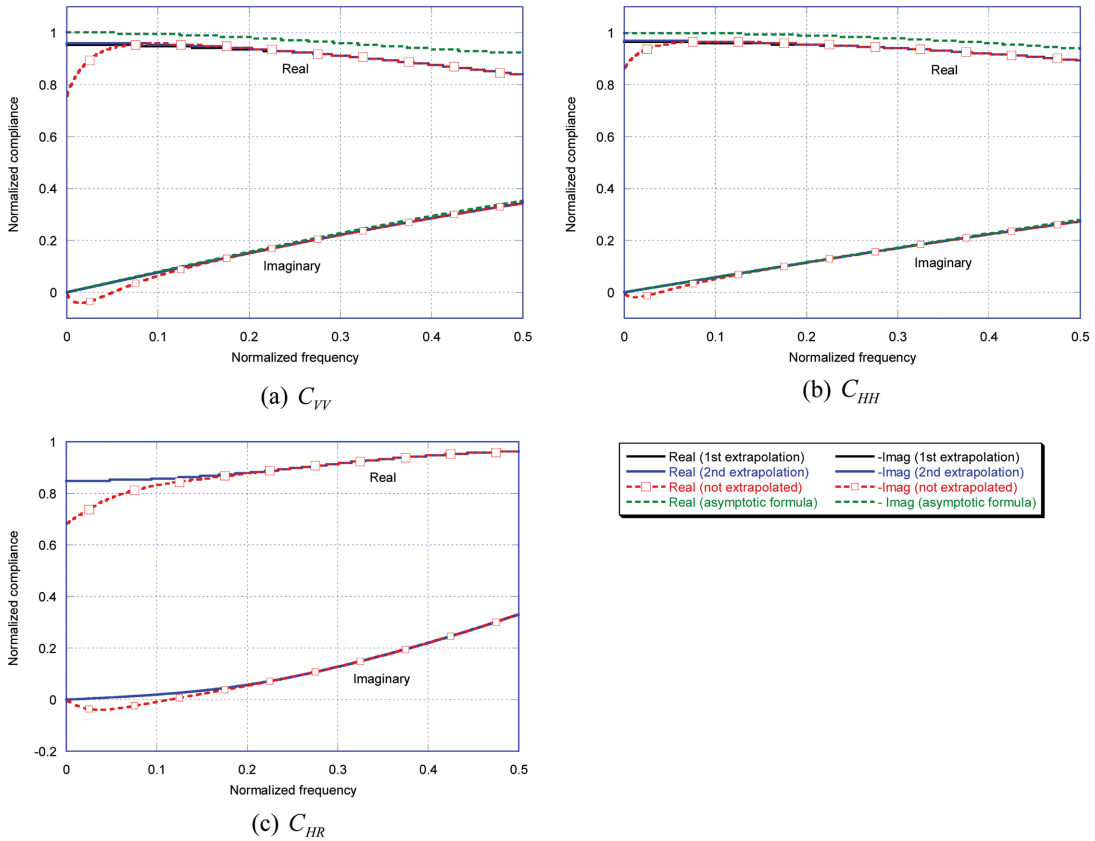

(a) C_{VV} (b) C_{HH}

(c) C_{HR}

Fig. 10 Extrapolated compliance functions of a surface circular foundation

coefficients $A_{TT,0}$, $A_{TT,2}$, $A_{TT,3}$ and $A_{TT,5}$ are determined so that $C_{TT}^{e} = C_{TT}$ and $dC_{TT}^{e}/da_0 = dC_{TT}/da_0$ at $a_0 = a_0^e$.

Both extrapolation methods are applied to the problem of the surface circular foundation. The user-defined frequency a_0^e is taken as $0.08\pi = 0.251$. Since asymptotic expressions for the coupling compliance (C_{HR}) or stiffness (K_{HR}) are not available, the first extrapolation approach is applicable only to the diagonal entries of the compliance or stiffness matrices. Extrapolated results for the

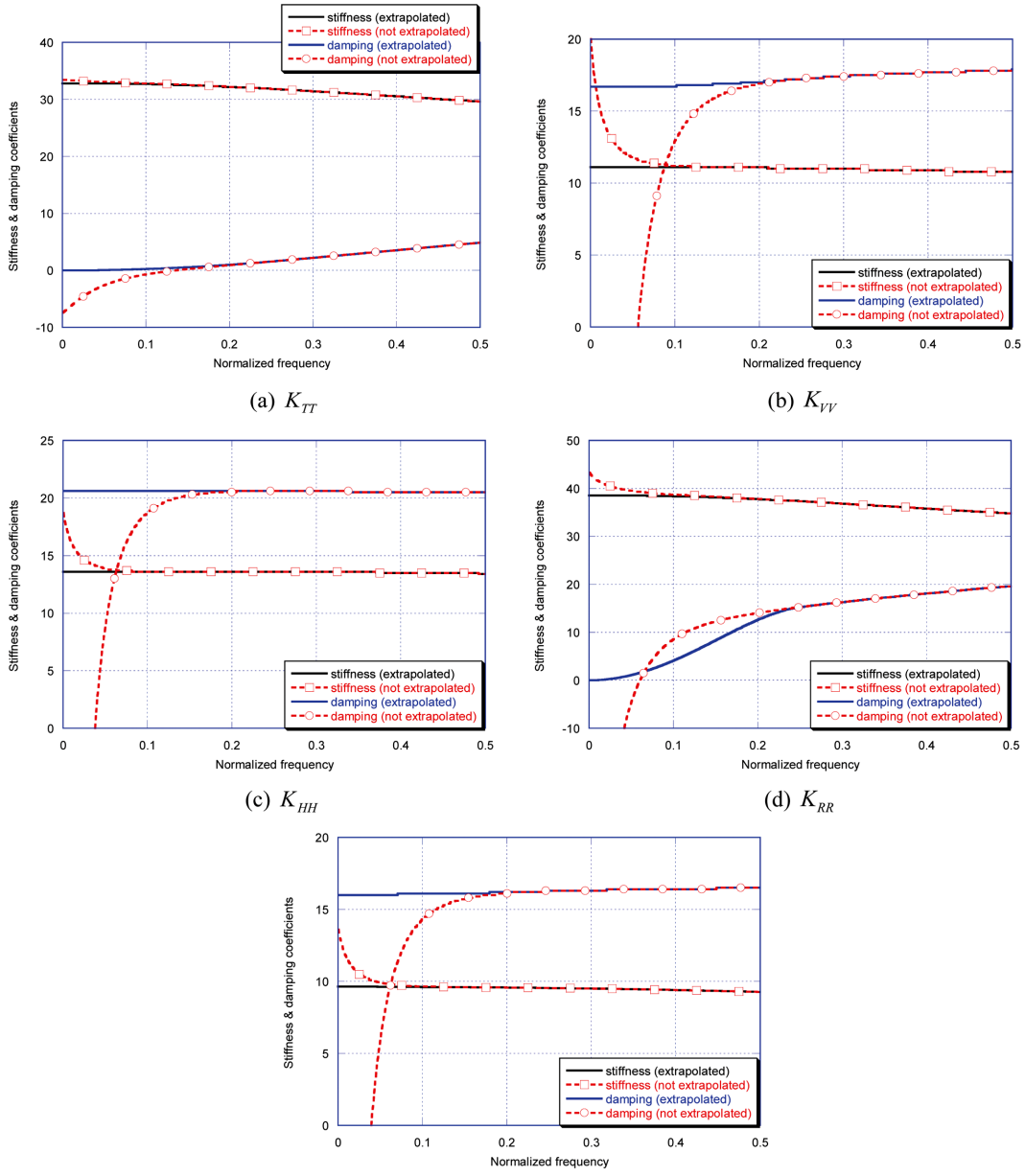

(a) K_{TT} (b) K_{VV}

(c) K_{HH} (d) K_{RR}

(e) K_{HR}

Fig. 11 Extrapolated impedance functions of an embedded cylindrical foundation

vertical, horizontal, and coupling compliances are shown in Fig. 10. It can be observed that the extrapolated results from both methods show substantial improvement.

The second extrapolation method is applied to the problem of an embedded cylindrical foundation with $E = 2R$ for which asymptotic expressions are not available. The user-defined frequency a_0^e is taken as $0.08\pi = 0.251$ in this case as well and the extrapolated results for the torsional, vertical, horizontal, rocking and coupling motions are shown in Fig. 11. Again, improved extrapolated results can be seen in the very-low-frequency range and for the static condition.

It can be concluded from the above discussion that using the two proposed extrapolation methods, the numerical method presented in the previous sections can be improved to give satisfactory results in the very-low-frequency range and for the static condition.

5. Conclusions

Impedance (and compliance) functions and foundation input motions of rigid cylindrical (or circular) foundations in a layered half-space were obtained in this study using a consistent transmitting boundary combined with continued-fraction absorbing boundary conditions. The effects of obliquely incident seismic waves in a layered half-space were taken into account in the formulation of the transmitting boundary. Impedance (and compliance) functions and input motions of rigid circular foundations on the surface of or embedded in a homogeneous half-space were computed and compared with available results. Extrapolation methods were proposed for improvement of the results in the very-low-frequency range and for the static condition. It can be concluded from the applications that accurate analysis of foundation dynamics and soil-structure interaction in a layered half-space can be carried out by the presented numerical method.

Acknowledgements

This work was supported by the National Research Foundation of Korea Grant funded by the Korean Government [NRF-2009-352-D00292].

References

Andrade, P.W. (1999), *Implementation of second-order absorbing boundary conditions in frequency-domain computations*, Ph.D. Dissertation, The University of Texas at Austin, Texas.

Apsel, R.J. and Luco, J.E. (1987), "Impedance functions for foundations embedded in a layered medium: an integral equation approach", *Earthq. Eng. Struct. D.*, **15**(2), 213-231.

Bougacha, S., Tassoulas, J.L. and Roësset, J.M. (1993a), "Analysis of foundations on fluid-filled poroelastic stratum", *J. Eng. Mech.-ASCE*, **119**(8), 1632-1648.

Bougacha, S., Tassoulas, J.L. and Roësset, J.M. (1993b), "Dynamic stiffness of foundations on fluid-filled poroelastic stratum", *J. Eng. Mech.-ASCE*, **119**(8), 1649-1662.

Day, S.M. (1977), *Finite element analysis of seismic scattering problems*, PhD Dissertation, Univ. of California, San Diego, La Jolla, California.

Gazetas, G. and Roësset, J.M. (1976), "Forced vibrations of strip footings on layered soil", *Method. Struct. Anal.-ASCE*, **1**, 115-131.

Gazetas, G. and Roësset, J.M. (1979), "Vertical vibration of machine foundations", *J. Geotech. Eng. Div.-ASCE*, **105**(12), 1435-1454.
Gladwell, G.M.L. (1968), "Forced tangential and rotator vibration of a rigid circular disc on a semi-infinite solid", *Int. J. Eng. Sci*., **6**(10), 591-607.
Guddati, M.N. (2006), "Arbitrarily wide-angle wave equations for complex media", *Comput. Method. Appl. M.. Eng*., **195**(1-3), 65-93.
Iguchi, M. (1984), "Earthquake response of embedded cylindrical foundations to SH and SV waves", *Proceedings of the 8th World Conference of Earthquake Engineering*, San Francisco.
Kausel, E. (1974), *Forced vibrations of circular foundations on layered media*, Research Report R74-11, Department of Civil Engineering, Massachusetts Institute of Technology, Cambridge, Massachusetts.
Kausel, E. (1996), "Discussion: Dynamic response of a multi-layered poroelastic medium by Rajapakse R.K.N.D and Senjuntichai, T.", *Earthq. Eng. Struct. D*., **25**(10), 1165-1167.
Kausel, E., Roësset, J.M. and Waas, G. (1975), "Dynamic analysis of footings on layered media", *J. Eng. Mech. Div.-ASCE*, **101**(5), 679-693.
Kausel, E. and Roësset, J.M. (1975), "Dynamic stiffness of circular foundations", *J. Eng. Mech. Div.-ASCE*, **101**(6), 771-785.
Lee, J.H, Kim, J.K. and Tassoulas, J.L. (2011a), "Implementation of a second-order paraxial boundary condition for a water-saturated layered half-space in plane strain", *Earthq. Eng. Struct. D*., **40**(5), 531-550.
Lee, J.H., Kim, J.K. and Tassoulas, J.L. (2011b), "Application of a second-order paraxial boundary condition to the problems of dynamics of circular foundations on a porous layered half-space", *Soil Dyn. Earthq. Eng*., **31**(3), 291-305.
Lee, J.H. and Tassoulas, J.L. (2011), "Consistent transmitting boundary with continued-fraction absorbing boundary conditions for analysis of soil–structure interaction in a layered half-space", *Comput. Method. Appl. Mech. Eng*., **200**(13-16), 1509-1525.
Lin, H.T., Roësset, J.M. and Tassoulas, J.L. (1987), "Dynamic interaction between adjacent foundations", *Earthq. Eng. Struct. D*., **15**(3), 323-343.
Luco, J.E. (1982), "Linear soil-structure interaction: a review", in: Datta, S.K. (eds.), *Earthquake ground motion and its effects on structures*, AMD-vol. 53, ASME, New York, 41-57.
Luco, J.E. and Mita, A. (1987), "Response of a circular foundation on a uniform half-space to elastic waves", *Earthq. Eng. Struct. D*., **15**(1), 105-118.
Luco, J.E. and Westmann, R.A. (1971), "Dynamic response of circular footings", *J. Eng. Mech. Div.-ASCE*, **97**(5), 1381-1395.
Luco, J.E. and Westmann, R.A. (1972), "Dynamic response of a rigid footing bonded to an elastic half space", *J. Appl. Mech. ASME*, **39**, 527-541.
Luco, J.E. and Wong, H.L. (1987), "Seismic response of foundations embedded in a layered half-space", *Earthq. Eng. Struct. D*., **15**(2), 233-247.
Pais, A.L. and Kausel, E. (1989), "On rigid foundations subjected to seismic waves", *Earthq. Eng. Struct. D*., **18**(4), 475-489.
Robertson, I.A. (1966), "Forced vertical vibration of a rigid circular disc on a semi-infinite elastic solid", *Proc. Camb. Phil. Soc*., **62**(3), 547-553.
Roësset, J.M. (1980), "A review of soil-structure interaction", *Report UCRL-15262*, Seismic Safety Margins Research Program, Lawrence Livermore Laboratory.
Tassoulas, J.L. (1981), *Elements for the numerical analysis of wave motion in layered media*, Research Report R81-2, Department of Civil Engineering, Massachusetts Institute of Technology, Cambridge, Massachusetts.
Tassoulas, J.L. (1984), "An investigation of the effect of the rigid sidewall on the response of embedded circular foundations to obliquely incident SV- and P-waves", *Int. Symp. Dyn. Soil Struct. Interact*., Minneapolis, 4-5 September, 55-64.
Thomas, D.P. (1968), "A note on the torsional oscillations of an elastic half space", *Int. J. Eng. Sci*., **6**(10), 565-570.
Waas, G. (1972), *Linear two-dimensional analysis of soil dynamics problems in semi-infinite layered media*, Ph.D. Dissertation, University of California, Berkeley, California.
Wong, H.L. (1975), *Dynamic soil-structure interaction*, Report EERL-75-01, Earthquake Engineering Research

Laboratory, California Institute of Technology, Pasadena, California.
Wong, H.L. and Luco, J.E. (1978a), *Tables of impedance functions and input motions for rectangular foundations*, Report CE 78-15, Department of Civil Engineering, University of Southern California, Los Angeles, California.
Wong, H.L. and Luco, J.E. (1978b), "Dynamic response of rectangular foundations to obliquely incident seismic waves", *Earthq. Eng. Struct. D*., **6**(1), 3-16.

SA

Appendix. Asymptotic behaviors of a rigid circular foundation on the surface of a homogeneous half-space

Asymptotic behaviors at low frequency for a rigid circular foundation on the surface of a homogeneous half-space are summarized. An expression for the torsional motion is given by Thomas (1968), for the vertical motion by Robertson (1966), for the horizontal and rocking motions by Galdwell (1968)

For the torsional motion

$$C_{TT} = \frac{3}{16\mu R^3}\left\{\left[1+\frac{1}{5}a_0^2-\frac{34}{525}a_0^4+\cdots\right]+i\left[-\frac{4}{9\pi}a_0^3+\frac{16}{225\pi}a_0^5+\cdots\right]\right\} \tag{A1a}$$

$$K_{TT} = \frac{16\mu R^3}{3}\left\{\left[1-\frac{1}{5}a_0^2+\frac{11}{105}a_0^4+\cdots\right]+i\left[\frac{4}{9\pi}a_0^3-\frac{56}{225\pi}a_0^5+\cdots\right]\right\} \tag{A1b}$$

For the vertical motion

$$C_{VV} = \frac{1-v}{4\mu R}\left\{\left[1-\frac{2I_2}{3\pi}a_0^2-\frac{-120\pi^3 I_4+204\pi^2 I_1 I_3+19\pi^2 I_2^2+720 I_1^4-960\pi I_1^2 I_2}{180\pi^4}a_0^4+\cdots\right]\right.$$
$$\left.+i\left[-\frac{I_1}{\pi}a_0-\frac{\pi^2 I_3-8\pi I_1 I_2+6I_1^3}{3\pi^3}a_0^3+\cdots\right]\right\} \tag{A2a}$$

$$K_{VV} = \frac{4\mu R}{1-v}\left\{\left[1+\frac{2\pi I_2-3I_1^2}{3\pi^2}a_0^2+\frac{-40\pi^3 I_4+28\pi^2 I_1 I_3+33\pi^2 I_2^2+60 I_1^4-120\pi I_1^2 I_2}{60\pi^4}a_0^4+\ldots\right]\right.$$
$$\left.+i\left[\frac{I_1}{\pi}a_0-\frac{\pi^2 I_3-4\pi I_1 I_2+3I_1^3}{3\pi^3}a_0^3+\cdots\right]\right\} \tag{A2b}$$

For the horizontal motion

$$C_{HH} = \frac{2-v}{8\mu R}\left\{\left[1-\frac{1}{3}B_2 a_0^2+\cdots\right]+i\left[-B_1 a_0+\frac{2}{3}B_3 a_0^3+\cdots\right]\right\} \tag{A3a}$$

$$K_{HH} = \frac{8\mu R}{2-v}\left\{\left[1+\left(\frac{1}{3}B_2-B_1^2\right)a_0^2+\cdots\right]+i\left[B_1 a_0+\left(-\frac{2}{3}B_3+\frac{2}{3}B_1 B_2-B_1^3\right)a_0^3+\cdots\right]\right\} \tag{A3b}$$

For the rocking motion

$$C_{RR} = \frac{3(1-v)}{8\mu R^3}\left\{\left[1+\frac{2I_2}{5\pi}a_0^2-\frac{90\pi I_4+I_2^2}{525\pi^2}a_0^4+\cdots\right]+i\left[-\frac{I_3}{3\pi}a_0^3+\frac{I_5}{15\pi}a_0^5+\cdots\right]\right\} \tag{A4a}$$

$$K_{RR} = \frac{8\mu R^3}{3(1-v)}\left\{\left[1-\frac{2I_2}{5\pi}a_0^2+\frac{18\pi I_4+17I_2^2}{105\pi^2}a_0^4+\cdots\right]+i\left[\frac{I_3}{3\pi}a_0^3-\frac{\pi I_5+4I_2I_3}{15\pi^2}a_0^5+\cdots\right]\right\} \tag{A4b}$$

The constants I_1, I_2, etc. in Eqs. (A2) and (A4) are defined and their numerical values are given by Robertson (1966). The constants B_1, B_2 and B_3 in Eq. (A3) are defined by Galdwell (1968).